Supporting Information

An *in situ* growth route towards anti-perovskite Ni_3InN nanoparticles embedded within amorphous silicon nitride

Shotaro Tada,[a, d] Sakurako Takazawa,[a] Norifumi Asakuma,[a] Maxime Cheype,[b] Sawao Honda,[a] Ravi Kumar[c], Samuel Bernard,[b] and Yuji Iwamoto[*a]

a. Department of Life Science and Applied Chemistry, Graduate School of Engineering, Nagoya Institute of Technology, Gokiso-cho, Showa-ku, Nagoya 466-8555, Japan
b. University of Limoges, CNRS, IRCER, UMR 7315, F-87000, Limoges, France
c. Laboratory for High Performance Ceramics, Department of Metallurgical and Materials Engineering, Indian Institute of Technology Madras (IIT Madras), Chennai 600036, India
d. Department of Metallurgical and Materials Engineering, Indian Institute of Technology Madras (IIT Madras), Chennai 600036, India

* Corresponding author: Yuji Iwamoto
E-mail: iwamoto.yuji@nitech.ac.jp
Tel/Fax: +81-52-735-5276

Keywords
Anti-perovskite, Ni_3InN, amorphous silicon nitride, polymer-derived ceramics (PDCs)

1. Synthesis of $Ni_{0.1}In_{0.1}$-PH sample

The handling of the chemicals and reagents was performed under an inert atmosphere of pure argon (Ar) using standard Schlenk techniques and vacuum/Ar lines. Commercially available perhydropolysilazane (PHPS, NN120-20, 20 wt% in dibutyl ether solution) was provided by Sanwa Kagaku, Corp., Shizuoka, Japan. The dibutyl ether was substituted by super-anhydrous toluene (99.5 % purity, Wako Pure Chemical Industries, Ltd., Osaka, Japan) to be 20 wt% for the PHPS contents.

In a typical experiment for **$Ni_{0.1}In_{0.1}$-PH** sample, a 100 mL two-neck round-bottom flask equipped with a magnetic stirrer was charged with the solvent-substituted PHPS (10 mL, 44 mmol, 20 wt% in toluene) and toluene (30 mL), then $NiCl_2$ (0.59 g, 4.4 mmol, Ni/Si = 0.1) and $InCl_3$ (0.98 g, 4.4 mmol, In/Si = 0.1) were added to the solution at room temperature. The reaction mixture was vigorously stirred at R.T. for 30 min and subsequently refluxed at 110 °C for 15 h under flowing Ar with maintaining vigorous stirring. After the reaction mixture was cooled to room temperature, the toluene solvent was removed under vacuum at 60 °C to give a **$Ni_{0.1}In_{0.1}$-PH** sample.

2. Supporting data

Scheme S1 Dehydrogenation reaction of Si-H/N-H in PSZ catalyzed by $NiCl_2$ and possible Ni(II) coordination structures such as 4-coordinate Ni(II) complex.

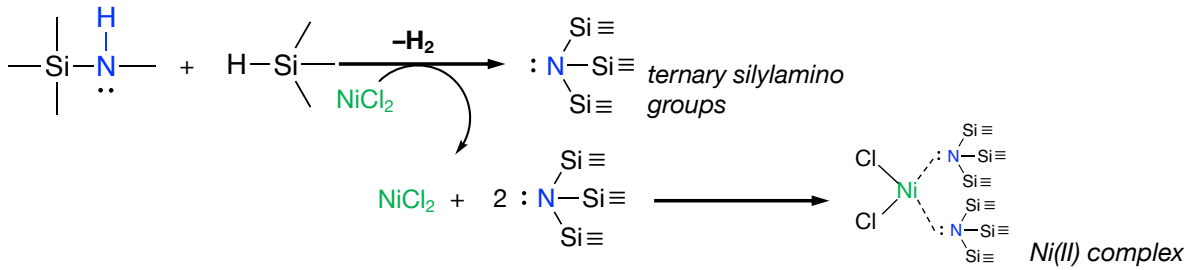

Table S1 The selected absorption bands position, band shift and relative intensity to νSi–N–Si ($I_{band}/I_{Si\text{-}N\text{-}Si}$) in the ATR-FTIR spectra for **$Ni_xIn_{0.1}$-DRZ** samples.

Band	Sample	Wavenumber	Band shift	Relative intensity
-	-	/cm^{-1}	/cm^{-1}	(I_{band} / $I_{Si\text{-}N\text{-}Si}$)
ν(Si-N-Si)	Durazane®1800	881.3	-	1
	$In_{0.1}$-DRZ	876.5	-4.82	1
	$Ni_{0.05}In_{0.1}$-DRZ	880.4	-0.96	1
	$Ni_{0.1}In_{0.1}$-DRZ	881.3	0	1
ν(N-H)	Durazane®1800	3378.7	-	0.237
	$In_{0.1}$-DRZ	3400.9	22.2	0.157
	$Ni_{0.05}In_{0.1}$-DRZ	3398.0	19.3	0.092
	$Ni_{0.1}In_{0.1}$-DRZ	3398.9	20.2	0.091
ρ(Si_2N-H)	Durazane®1800	1160.9	-	0.508
	$In_{0.1}$-DRZ	1133.0	-27.9	0.244
	$Ni_{0.05}In_{0.1}$-DRZ	1140.7	-20.2	0.158
	$Ni_{0.1}In_{0.1}$-DRZ	1133.0	-27.9	0.133
ν(Si-H)	Durazane®1800	2121.3	-	0.241
	$In_{0.1}$-DRZ	2123.2	1.9	0.163
	$Ni_{0.05}In_{0.1}$-DRZ	2128.1	6.8	0.102
	$Ni_{0.1}In_{0.1}$-DRZ	2130.0	8.7	0.068
δ(Si-CH_3)	Durazane®1800	1253.5	-	0.278
	$In_{0.1}$-DRZ	1254.5	1	0.329
	$Ni_{0.05}In_{0.1}$-DRZ	1256.4	2.9	0.321
	$Ni_{0.1}In_{0.1}$-DRZ	1259.3	5.8	0.354
δ(C–H, Vinyl)	Durazane®1800	1403.9	-	0.058
	$In_{0.1}$-DRZ	1403.0	-0.9	0.109
	$Ni_{0.05}In_{0.1}$-DRZ	1403.0	-0.9	0.087
	$Ni_{0.1}In_{0.1}$-DRZ	1403.0	-0.9	0.120

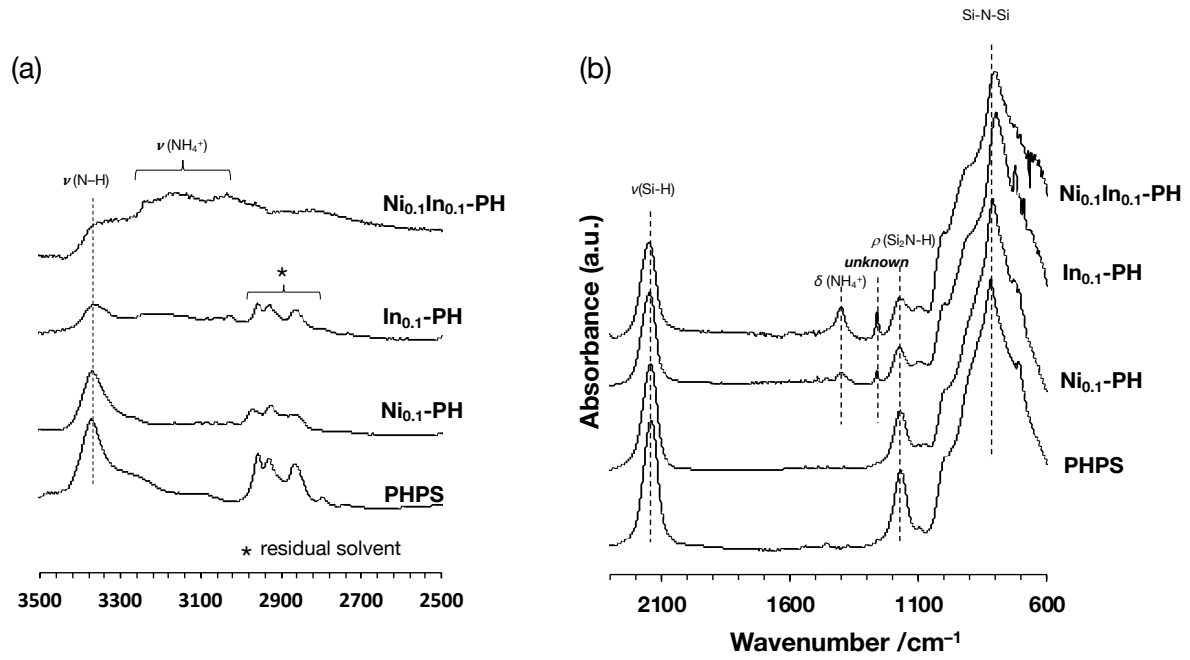

Fig. S1 ATR-FTIR spectra of as-synthesized **Ni_xIn_y-PH** samples in the range of (a) 3500–2500 cm^{-1} and (b) 2300–600 cm^{-1}.

[FTIR analysis]

As reference spectra, as-received PHPS was recorded. FTIR (ATR /cm^{-1}): 3373 (νN–H), 2143 (νSi–H), 1172 (ρSi_2N-H) and 822 (νSi–N–Si) [1-5]. The νSi–N–Si stretching bands for $NiCl_2$ and $InCl_3$-*co*-modified PHPS samples indicated all lower wavenumber (WN) values than those for as-received PHPS sample. The absorption band shift of the νSi–N–Si on **$Ni_{0.1}$-PH**, **$In_{0.1}$-PH**, and **$Ni_{0.1}In_{0.1}$-PH** samples were measured to be –7.7, –22.2, and –20.3 cm^{-1}, respectively. It was found that the extent of band shift is greater in **$In_{0.1}$-PH** and **$Ni_{0.1}In_{0.1}$-PH** samples compared to the **$Ni_{0.1}$-PH** sample. In addition, the chemical modification of PHPS with $NiCl_2$ and $InCl_3$ resulted in a reduction of the relative intensity on both ρSi_2N-H and νSi–H bands. The extent of decreased intensities of both ρSi_2N-H and νSi–H was greater for **$In_{0.1}$-PH** and **$Ni_{0.1}In_{0.1}$-PH** samples compared to **$Ni_{0.1}$-PH** sample. The νSi–H stretching band varies toward higher WN values in the range 2142–2152 cm^{-1}. The vibrational frequency of the νSi–H increases either through the electronegativity (***X***) of the substituting group increases [6] or through the increase of nitrogen concentration within the precursors [7], *i.e.*, the substitution of H atoms (***X*** = 2.2 by Pauling scale) with N atoms (***X*** = 3.0 by Pauling scale) on Si atoms back bonded to Si–H bonds. The substitution leads to the νSi–H stretching mode toward higher

frequency due to the induction effect. This result is consistent with the formation of the ternary silylamino group during reflux at 110 °C. Additionally, new absorption bands appeared on **$In_{0.1}$-PH** and **$Ni_{0.1}In_{0.1}$-PH** samples (**Fig. S1a**) at 3240, 3150, and 1404 cm^{-1}, which are assigned to ammonium salt, most probably ammonium chloride (NH_4Cl) [8].

Reference:

1. O. Funayama, T. Kato, Y. Tashiro and T. Isoda, Synthesis of a Polyborosilazane and Its Conversion into Inorganic Compounds, *J. Am. Ceram. Soc.*, 1993, **76**, 717–723.
2. O. Funayama, Y. Tashiro, T. Aoki and T. Isoda, Synthesis and pyrolysis of polyaluminosilazane, *Nippon Seramikkusu Kyokai Gakujutsu Ronbunshi/Journal Ceram. Soc. Japan*, 1994, **102**, 908–912.
3. Y. Iwamoto, K. Kikuta and S. Hirano, Microstructural development of Si_3N_4 –SiC–Y_2O_3 ceramics derived from polymeric precursors, *J. Mater. Res.*, 1998, **13**, 353–361.
4. Y. Iwamoto, K. Kikuta and S. Hirano, Si_3N_4 –SiC–Y_2O_3 ceramics derived from yttrium-modified block copolymer of perhydropolysilazane and hydroxy-polycarbosilane, *J. Mater. Res.*, 1999, **14**, 1886–1895.
5. Y. Iwamoto, K. Kikuta and S. Hirano, Si_3N_4–TiN–Y_2O_3 ceramics derived from chemically modified perhydropolysilazane, *J. Mater. Res.*, 1999, **14**, 4294–4301.
6. G. Lucovsky, R. J. Nemanich and J. C. Knights, Structural interpretation of the vibrational spectra of a-Si: H alloys, *Phys. Rev. B*, 1979, **19**, 2064–2073.
7. I. V. Afanasyev-Charkin, L. G. Jacobsohn, R. D. Averitt and M. Nastasi, Amorphous silicon nitride films of different composition deposited at room temperature by pulsed glow discharge plasma immersion ion implantation and deposition, *J. Vac. Sci. Technol. A Vacuum, Surfaces, Film.*, 2004, **22**, 2342–2346.
8. Q. Qu, L. Li, W. Bai, C. Yan and C. N. Cao, Effects of NaCl and NH_4Cl on the initial atmospheric corrosion of zinc, *Corros. Sci.*, 2005, **47**, 2832–2840.

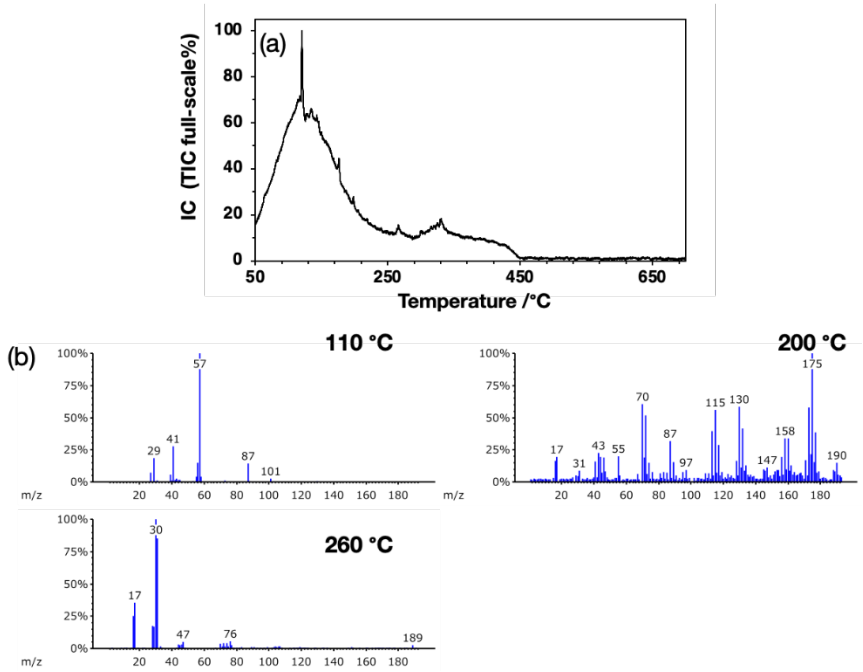

Fig. S2 TG-MS analysis of PHPS: (a) The total ion current (TIC) chromatogram and (b) mass fragments at selected temperatures.

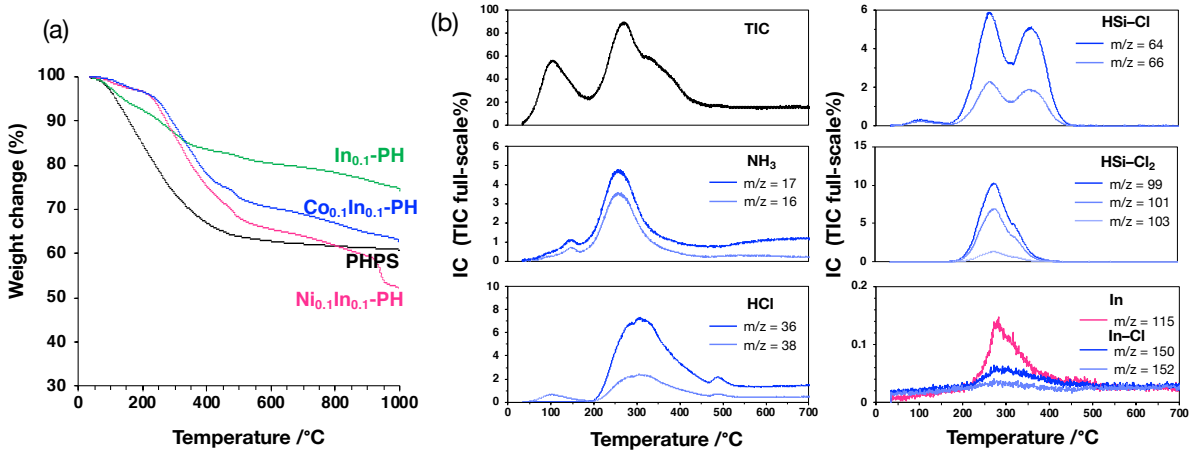

Fig. S3 (a) TG-curves of starting PHPS and as-synthesized $\mathbf{M_xIn_{0.1}}$**-PH** samples (M = Ni and Co, x = 0 or 0.1) to 1000 °C under He and (b) the total ion current (TIC) chromatogram and selected mass fragments measured for $\mathbf{Ni_{0.1}In_{0.1}}$**-PH** sample during TG-MS analysis.

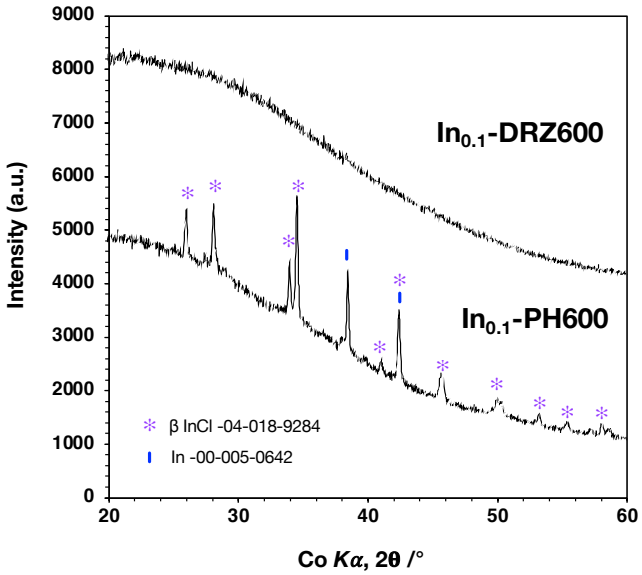

Fig. S4 XRD patterns of (a) **$In_{0.1}$-PH600** and (b) **$In_{0.1}$-DRZ600** samples

[TG-MS analysis]

The TG-curve of as-received PHPS (**Fig. S3a**) displays a weight loss at 50–550 °C, resulting in a final ceramic yield of 60.9 %. According to the MS analyses of as-received PHPS (**Fig. S3b**), these weight losses are due to the volatilization of residual solvents such as dibutyl ether (mass spectra measured at 110 °C, m/z = 57, 41, 29), low molecular weight organosilicon compounds such as ≡Si–NH– (mass spectra measured at 200 °C, m/z = 43) and NH_3 (m/z = 17), which are associated with cross-linking reactions of the precursor through trans-amination, and bond redistribution reactions.

The **$Ni_{0.1}In_{0.1}$-PH and $Co_{0.1}In_{0.1}$-PH** samples showed similar behavior of weight loss (**Fig. S3a**). The weight loss at 50-300 °C was significantly suppressed compared to the as-received PHPS. As discussed in the FTIR results (**Fig. S1**), the catalytic cross-linking reaction of the PSZ network during polymer synthesis through the dehydrocoupling reaction of Si-H/N-H catalyzed by MCl_2 helps to suppress the weight loss in this temperature range. In contrast to **$M_{0.1}In_{0.1}$-PH** samples, the **$In_{0.1}$-PH** sample showed less pronounced weight loss suppression in this temperature range, possibly due to either the quantitative dependence or the participation of a different reaction—*i.e.*, acid-base reaction—for **$In_{0.1}$-PH** sample.

The weight loss from 330 °C to 500 °C is greater in **$Ni_{0.1}In_{0.1}$-PH** and **$Co_{0.1}In_{0.1}$-PH** samples, indicating the volatilization of $InCl_3$ which usually starts at 330 °C under an inert atmosphere [1]. There was no significant difference in the weight loss of **$Ni_{0.1}In_{0.1}$-PH** and **$Co_{0.1}In_{0.1}$-PH** samples, with the difference being within about 5% at 550 °C; however, the Co

species showed a smaller weight loss. In contrast, the **$In_{0.1}$-PH** sample showed a featureless slope in this temperature range, suggesting that the in situ formation of In–N bond via acid-base reaction during synthesis reduced the amount of unreacted $InCl_3$ which evaporated at around 330 °C. Weight loss from 550 °C is not observed in as-received PHPS but is observed in **$In_{0.1}$-PH**, **$Ni_{0.1}In_{0.1}$-PH** and **$Co_{0.1}In_{0.1}$-PH** samples suggesting that the decomposition of the in situ formed In-N bonds occurred over 550 °C under an inert atmosphere [2].

Reference:

1. C. Karakaya, S. Ricote, D. Albin, E. Sánchez-Cortezón, B. Linares-Zea and R. J. Kee, Thermogravimetric analysis of $InCl_3$ sublimation at atmospheric pressure, *Thermochim. Acta*, 2015, **622**, 55–63.
2. Q. Guo, O. Kato and A. Yoshida, Thermal stability of indium nitride single crystal films, *J. Appl. Phys.*, 1993, **73**, 7969–7971.

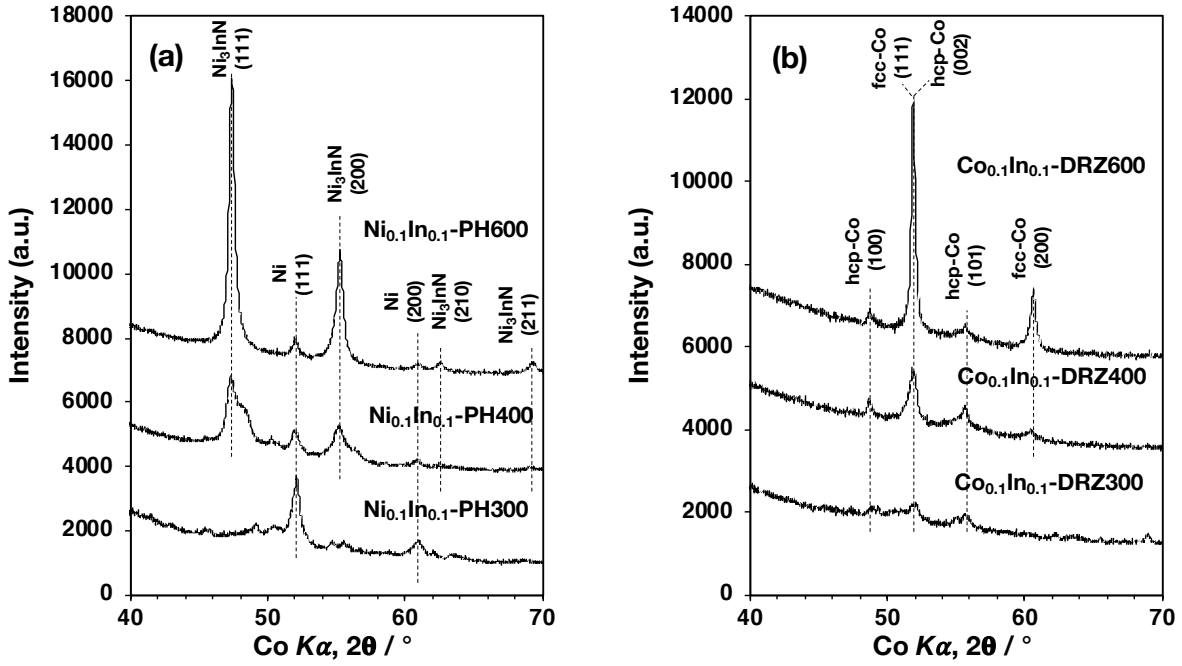

Fig. S5 XRD patterns of (a) **$Ni_{0.1}In_{0.1}$-PH*T*** and (b) **$Co_{0.1}In_{0.1}$-DRZ*T*** samples, ***T*** is pyrolysis temperatures (300, 400, and 600 °C).

Table S2 Chemical composition of as-pyrolyzed $Ni_{0.1}In_{0.1}$-PH*T* samples (*T* = 300, 400, and 600)

Name	Composition (wt%)							Atomic ratio normalized on Si
	Si	C	N	O	Ni	In	Cl	
$Ni_{0.1}In_{0.1}$-PH300	44.26	0.51	25.52	3.03	11.23	9.20	6.26	$Si_1N_{1.16}O_{0.12}Ni_{0.12}In_{0.05}Cl_{0.11}$
$Ni_{0.1}In_{0.1}$-PH400	45.44	0.43	27.96	2.76	10.79	7.26	5.36	$Si_1N_{1.23}O_{0.11}Ni_{0.11}In_{0.04}Cl_{0.09}$
$Ni_{0.1}In_{0.1}$-PH600	40.55	0.38	31.80	4.21	12.41	6.98	3.67	$Si_1N_{1.57}O_{0.18}Ni_{0.15}In_{0.04}Cl_{0.07}$

Table S3 Chemical composition of as-pyrolyzed $Co_{0.1}In_{0.1}$-DRZ*T* samples (*T* = 300, 400, and 600)

Name	Composition (wt%)							Atomic ratio normalized on Si
	Si	C	N	O	Co	In	Cl	
$Co_{0.1}In_{0.1}$-DRZ300	37.65	4.94	21.88	3.35	9.43	13.72	9.04	$Si_1C_{0.31}N_{1.17}O_{0.16}Co_{0.12}In_{0.09}Cl_{0.19}$
$Co_{0.1}In_{0.1}$-DRZ400	33.43	0.68	29.25	7.88	9.44	10.29	9.03	$Si_1C_{0.05}N_{1.75}O_{0.41}Co_{0.13}In_{0.08}Cl_{0.21}$
$Co_{0.1}In_{0.1}$-DRZ600	43.76	0.39	31.79	4.25	16.78	0.13	2.89	$Si_1C_{0.02}N_{1.46}O_{0.17}Co_{0.18}In_{0.00}Cl_{0.05}$

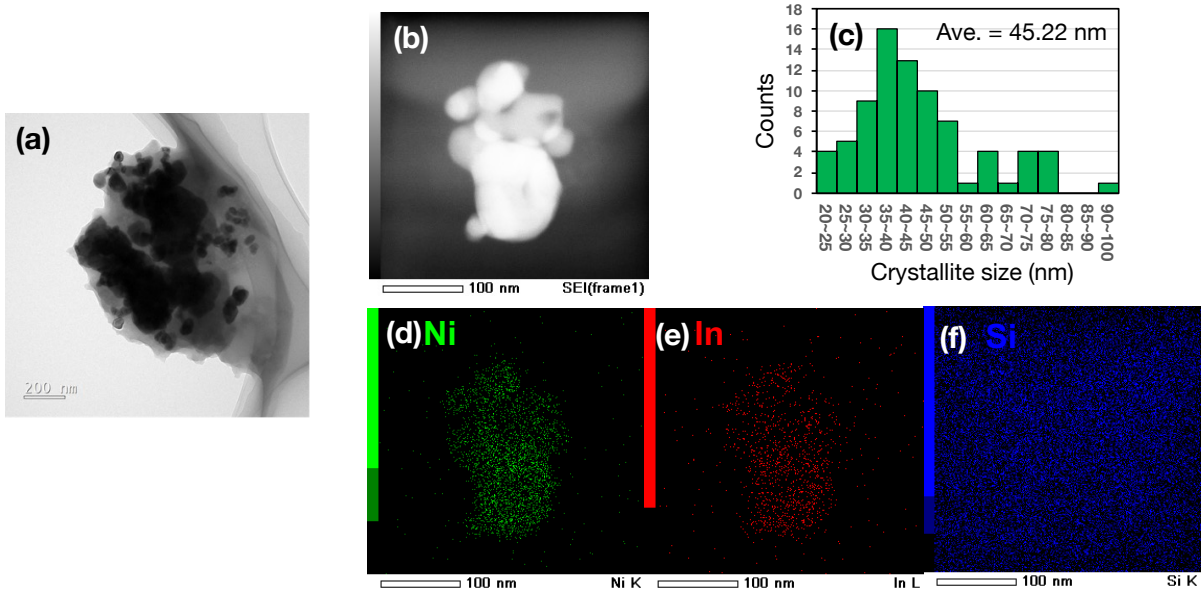

Fig. S6 (a) BF-TEM image and (b) HAADF-STEM image of the $Ni_{0.05}In_{0.1}$-DRZ600 sample. (c) the Ni_3InN crystallite size distribution, and the result of STEM-EDS mapping of (d) Ni, (e) In and (f) Si.

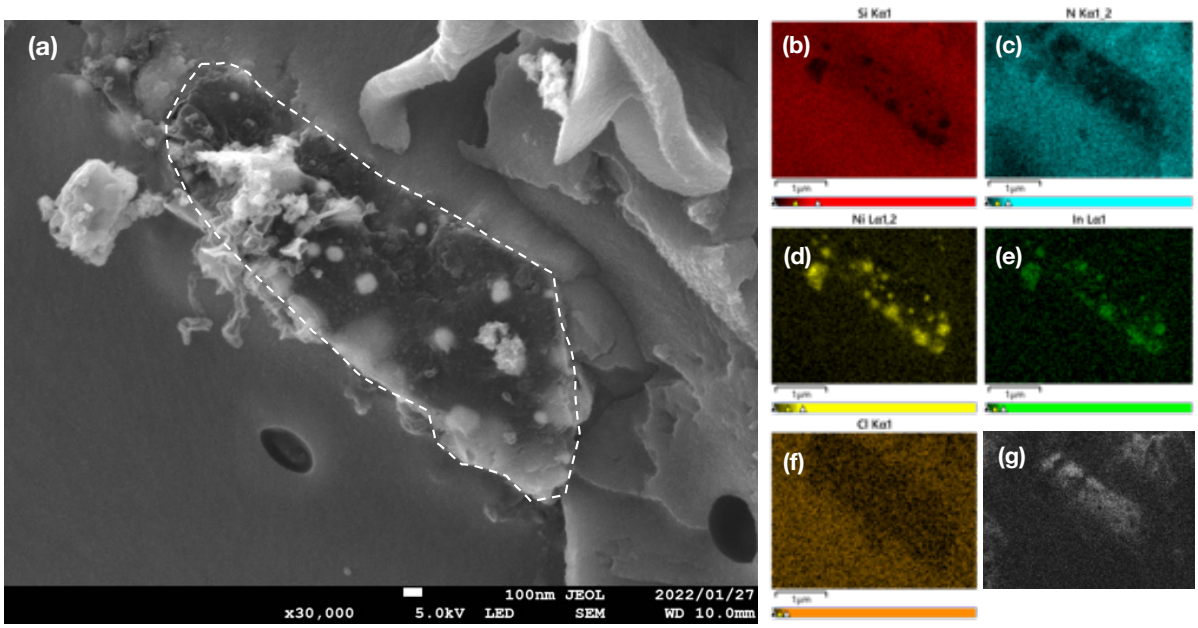

Fig. S7 SEM-EDS and SEM-CL image analysis for the **$Ni_{0.1}In_{0.1}$-PH600** sample: (a) SEM image, and the results of EDS mapping of (b) Si, (c) N, (d) Ni, (e) In, and (f) Cl. (g) the SEM-CL image of the selected area around the nanoparticles. The white dashed line represents the monolithic region of a-SiN matrix.

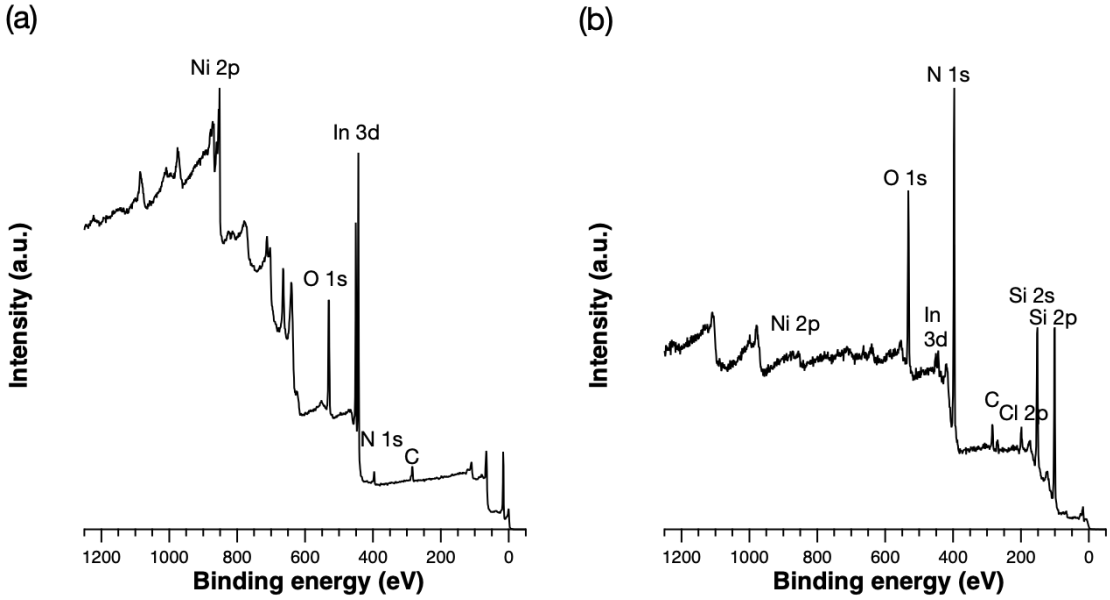

Fig. S8 XPS survey scan spectra for (a) bulk Ni_3InN and (b) Ni_3InN/SiN nanocomposite (**$Ni_{0.1}In_{0.1}$-PH600** sample)

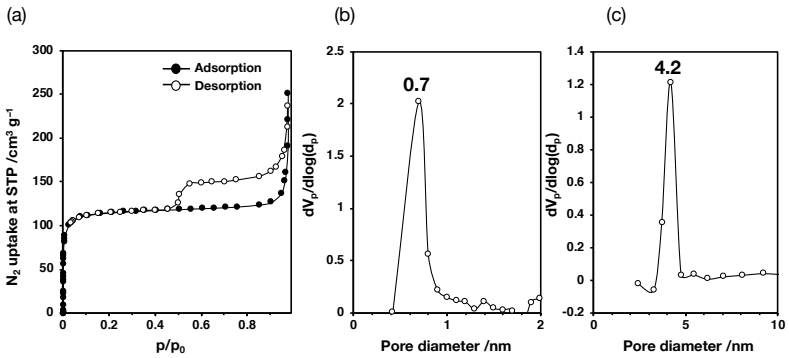

Fig. S9 (a) N_2 adsorption and desorption isotherms at –196 °C for **$Ni_{0.05}In_{0.1}$-DRZ600** sample, and the resulting pore size distribution curve characterized by the (b) MP plot and (c) BJH plot.

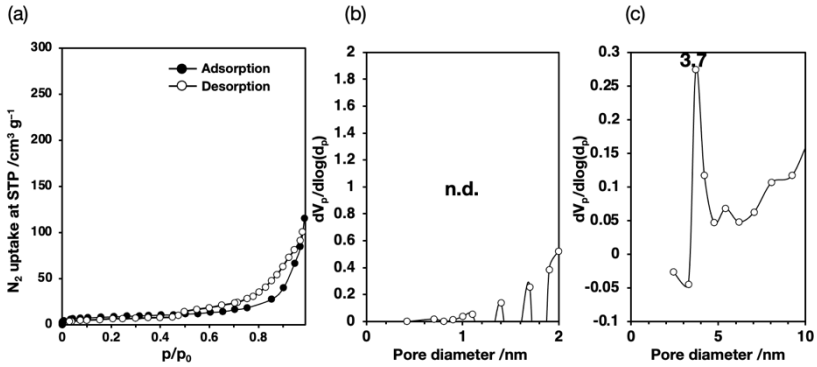

Fig. S10 (a) N_2 adsorption and desorption isotherms at –196 °C for **$Ni_{0.1}In_{0.1}$-PH600** sample, and the resulting pore size distribution curve characterized by the (b) MP plot and (c) BJH plot.

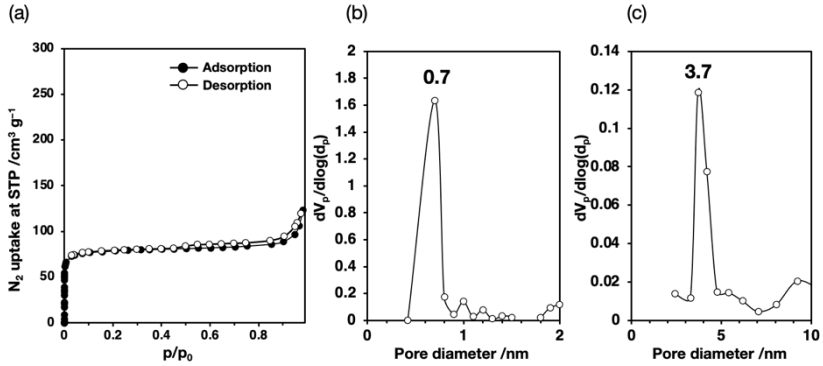

Fig. S11 (a) N_2 adsorption and desorption isotherms at –196 °C for **$Ni_{0.1}In_{0.1}$-DRZ600** sample, and the resulting pore size distribution curve characterized by the (b) MP and (c) BJH plot.

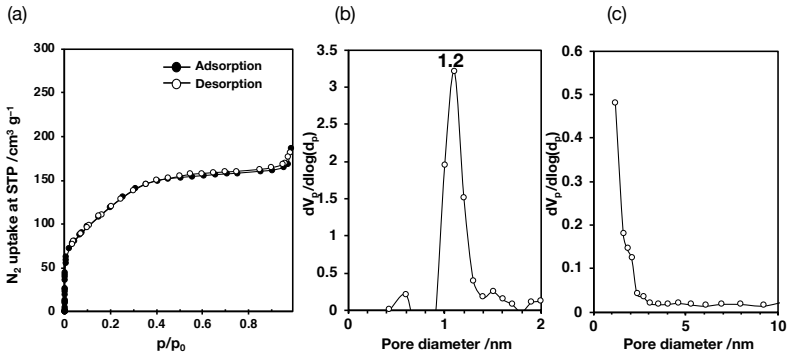

Fig. S12 (a) N_2 adsorption and desorption isotherms at –196 °C for **$In_{0.1}$-DRZ600**, and the resulting pore size distribution curve characterized by the (b) MP and (c) BJH plot.

Table S4 The Brunauer–Emmett–Teller (BET) surface areas and pore volumes of pyrolyzed samples.

Samples	S_{BET} /m^2 g^{-1}	$V_{BET, total}$ /cm^3 g^{-1}	V_{micro} /cm^3 g^{-1}	V_{meso} /cm^3 g^{-1}
$Ni_{0.1}In_{0.1}$-PH600	32	0.18	n.d.	0.17
$Ni_{0.05}In_{0.1}$-DRZ600	460	0.39	0.19	0.18
$Ni_{0.1}In_{0.1}$-DRZ600	315	0.19	0.13	0.08
$In_{0.1}$-DRZ600	441	0.29	0.24	n.d.